Dyes and Pigments 121 (2015) 1–6

Contents lists available at ScienceDirect

Dyes and Pigments

journal homepage: www.elsevier.com/locate/dyepig

Rationally designed non-enzymatic fluorogenic 'turn-on' probe for uric acid

Tuhin Pradhan [a, 1], Sukhendu Maiti [b, 1], Rajesh Kumar [b, 1], Yun Hak Lee [b], Jong Wan Kim [c], Joung Hae Lee [d, **], Jong Seung Kim [b, *]

[a] Department of Chemistry, Vel Tech Dr. RR & Dr. SR Technical University, Avadi, Chennai 600062, India
[b] Department of Chemistry, Korea University, Seoul 136-701, Republic of Korea
[c] Department of Laboratory Medicine, College of Medicine, Dankook University, Cheonan 330-715, Republic of Korea
[d] Korea Research Institute of Standards and Science, Daejon 305-600, Republic of Korea

ARTICLE INFO

Article history:
Received 11 March 2015
Received in revised form
30 April 2015
Accepted 3 May 2015
Available online 9 May 2015

Keywords:
Uric acid
Fluorescence
BODIPY
Non-enzymatic
PET
Hydrogen bonding

ABSTRACT

The simple and cost-effective detection of uric acid in serum or urine is highly desirable as uric acid acts as a biomarker for various diseases. Herein, we report a rationally designed, non-enzymatic probe for the detection of uric acid in serum samples over a wide range of concentrations (lower: ~60 μM, higher: ~700 μM and normal: ~120–380 μM) with 'turn-on' fluorogenic behaviour.

1. Introduction

In human biological fluids such as blood and urine, uric acid (UA) is the major metabolized product of the purine base of nucleic acids, adenine and guanine [1]. The normal concentration of UA in human urine is around 2 mM, which is maintained by its production and excretion from the body by various bio-processes [2]. The normal concentration of uric acid in blood or serum ranges between 120 and 380 μM [3]. Altered concentration levels of UA (hyperuricemia or hypouricemia) lead to various abnormalities, and hence, are indicative of many diseases such as gout [4], kidney disorder [5], arthritis and cardiovascular disease [6,7], Lesch–Nyhan syndrome [8,9], nephritis [10], hypertension, and type 2 diabetes [11,12]. Hyperuricemia was observed in lymphoma and leukaemia patients, resulting in potential damage to their kidneys. Therefore, monitoring elevated levels of UA in serum and urine is highly significant and desirable.

Currently, in medical laboratories, UA levels are monitored using an uricase enzymatic assay [13,14] and electrochemical techniques [15,16]. The uricase enzyme hydrolyses uric acid to allantoin (a water-soluble compound) and hydrogen peroxide [17,18], which are detected by direct or indirect methods that lead to development of colour compounds. However, strong interference from ascorbic acid present in large amounts in body fluids, the high cost of enzymes, and the need to precisely control the pH make these methods less viable for the accurate determination of UA levels [19]. Similarly, various electrochemical methods for UA analysis also suffer strong interference from ascorbic acid due to its similar oxidation potential, which makes it difficult to electrochemically differentiate between these two [20–22]. Although significant development has been made for sensing of UA using various non-enzymatic and enzymatic methods [23–25], there is a need to develop a non-enzymatic, non-invasive, reliable, and simple method that can be applied for the routine determination of UA. Fluorescence signalling, which involves translating molecular recognition into fluorescence signals, offers a promising alternative to existing methods because of its high detection sensitivity, and quick response time [26]. Among various fluorescence

* Corresponding author. Tel.: +82 2 3290 3143; fax: +82 2 3290 3121.
** Corresponding author.
E-mail addresses: ecljh@kriss.re.kr (J.H. Lee), jongskim@korea.ac.kr (J.S. Kim).
[1] These authors contributed equally.

http://dx.doi.org/10.1016/j.dyepig.2015.05.001
0143-7208/

mechanisms, fluorescence enhancement is usually preferred in order to observe a high signal output.

In the present work, we have designed, synthesized, and evaluated the BODIPY (boron-dipyrromethene)-based fluorogenic probe **8** (Fig. 1a, Scheme 1) for 'turn-on' detection of UA in serum. Probe **8** is highly selective for UA over ascorbic acid and other analytes present in the serum. The design of probe **8** is based on complementary H-bonding interactions between UA and the probe. Hydrogen bonding plays an essential role in the construction and maintaining of the three dimensional structure of many bio-logical molecules. Earlier synthetic receptors which selectively bind and recognize the barbiturate family of drugs through several hydrogen bonding [27]. Like barbiturate derivatives, uric acid also has several hydrogen bonding sites that make it a desirable guest for forming complementary H-bonds with suitable host. On the other hand, BODIPY derivatives having high quantum efficiency, long wavelength emission and excellent photostability, are good fluorogenic probes for specific analytes [28]. Therefore, introduction of a selective chelating unit into the BODIPY unit can make it suitable fluorogenic receptor for uric acid. The present manuscript utilizes the H-bonding interactions between probe **8** and UA to achieve high detection selectivity and specificity. So far, 'turn-on' fluorogenic detection of UA using a simple and effective method that can detect and discriminate UA from other analytes has not been reported. We believe that probe **8** will be valuable in clinical and pharmaceutical analysis of UA.

2. Experimental section

2.1. General synthetic materials and sample preparation

The chemicals used for the reactions were purchased from Aldrich, Acros Organics, Alfa-Aesar, Carbosynth, and TCI, and used as received. Analytical TLC was performed using Merck 60 F254 silica gel. For column chromatography, silica gel 60 (Merck, 0.063–0.2 mm) was used. ^{1}H and ^{13}C NMR spectra were measured using $CDCl_3$, CD_3OD and DMSO on Varian 300 and 400 MHz spectrometers and TMS as an internal reference. Thermo Scientific LTQ Orbitrap Mass Spectrometer was used to record the ESI-MS spectra. The blood serum samples were provided from Dankook University Hospital. The working solutions of compound **8** were prepared from their stock solutions (1.0 mM) in DMSO and all the spectra were recorded under physiological conditions (PBS buffer, pH 7.2, 37 °C). The 6 μM of compound **8** was used to measure absorption and fluorescence spectra using S-3100 (Scinco) spectrophotometer and RFPC-5301 spectrofluorometer (Shimadzu) at excitation wavelength of 475 nm with slit widths of 3 and 3 nm (excitation and emission, respectively).

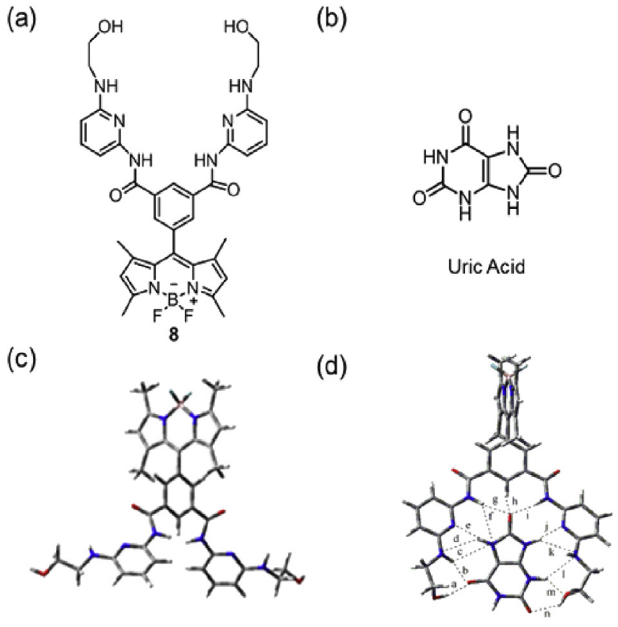

Fig. 1. Structure of (a) probe **8**, (b) uric acid. Optimized structure of (c) probe **8** and (d) **8**–uric acid, calculated using B3LYP/6-31G(d) level of theory. The red, blue, grey and white in molecular representation indicate oxygen, nitrogen, carbon and hydrogen atoms, respectively. Black dotted lines (a–n) in the **8**–uric acid complex indicate H-bonds. (For interpretation of the references to colour in this figure legend, the reader is referred to the web version of this article.)

2.2. Synthesis

2.2.1. Synthesis of 3,5-bis(methoxycarbonyl)benzoic acid (*2*)

Compound **2** was synthesized as per the reported procedure [29], yield: 55%.

^{1}H NMR ($CDCl_3$, 300 MHz): δ 4.01 (brs, 6H), 8.95 (brs, 3H). ^{13}C NMR ($CDCl_3$, 100 MHz): 53.3, 53.4, 131.4, 132.7, 133.7, 134.0, 134.3, 165.3, 166.2, 166.3 ppm. ESI-MS: Calculated for $C_{11}H_{10}O_6$ (M^+) 240.21; found 240.95.

2.2.2. Synthesis of dimethyl 5-(hydroxymethyl)isophthalate (*3*)

This compound was synthesized followed by reported procedure [29], yield: 45%.

^{1}H NMR ($CDCl_3$, 300 MHz): δ 3.94 (s, 6H), 4.81 (brs, 2H), 8.23 (brs, 2H), 8.58 (s, 1H). ^{13}C NMR ($CDCl_3$, 100 MHz): 52.7, 64.4, 130.0, 131.0, 132.2, 142.2, 166.4 ppm. ESI-MS: Calculated for $C_{11}H_{12}O_5$ 224.06; found 223.00 (M−1).

2.2.3. Synthesis of dimethyl 5-formylisophthalate (*4*)

A mixture of dimethyl 5-(hydroxymethyl)isophthalate (500 mg, 2.23 mmol), and 0.07 mL of HBr (48%) in DMSO (15 mL) was heated at 100 °C for 5 h in an oil bath. The reaction was monitored with TLC and after completion, the reaction mixture was diluted with ether and washed with brine. The solvent was evaporated under reduced pressure and reaction mixture was purified by column chromatography (Ether:Hexane 2:8–4:6) to afford compound **4** (80 mg, 16% yield) as a white solid. ^{1}H NMR ($CDCl_3$, 300 MHz): δ 3.92 (s, 6H), 8.61 (s, 2H), 8.80 (s, 2H), 10.05 (s, 1H). ^{13}C NMR ($CDCl_3$, 100 MHz): 52.9, 131.9, 134.4, 135.8, 137.0, 165.3, 190.5 ppm. HRMS: Calculated for $C_{11}H_{10}O_5$ 222.0528; found 223.0608 (M+1).

2.2.4. Synthesis of (Z)-dimethyl 5-((3,5-dimethyl-1H-pyrrol-2-yl)(3,5-dimethyl-2H-pyrrol-2-ylidene)methyl)isophthalate (*5*)

To a mixture of compound **4** (230 mg, 1.04 mmol) and 2,4-dimethylpyrrole (197 mg, 2.07 mmol) in 40 mL of CH_2Cl_2 solvent, a catalytic amount of TFA was added. The reaction mixture was stirred overnight at room temperature and monitored by TLC till consumption of the aldehyde. A solution of DDQ (307 mg, 1.35 mmol) was added and stirred for another 1 h. After completion, the reaction was quenched by adding water, CH_2Cl_2 layer was separated, evaporated under reduced pressure and purified by column chromatography on silica gel (EtOAc:Hexane 1:1–9:1) to give compound **5** (270 mg, 67% yield) as a blackish red sticky solid. ^{1}H NMR ($CDCl_3$, 300 MHz): δ 1.23 (s, 6H), 2.35 (s, 6H), 3.94 (s, 6H), 5.89 (s, 2H), 8.21 (s, 2H), 8.76 (s, 1H). HRMS: Calculated for $C_{23}H_{24}N_2O_4$ (M+1) 392.1736; found 393.1816.

2.2.5. Synthesis of 10-(3,5-bis(methoxycarbonyl)phenyl)-5,5-difluoro-1,3,7,9-tetramethyl-5H-dipyrrolo[1,2-c:1′,2′-f][1,3,2]diazaborinin-4-ium-5-uide (*6*)

Compound **5** (150 mg, 0.68 mmol) and DIPEA (1.8 mL, 10.2 mmol) were dissolved in 20 mL dichloromethane solvent and stirred at room temperature for 10 min. $BF_3{\cdot}OEt_2$ (1.45 mL,

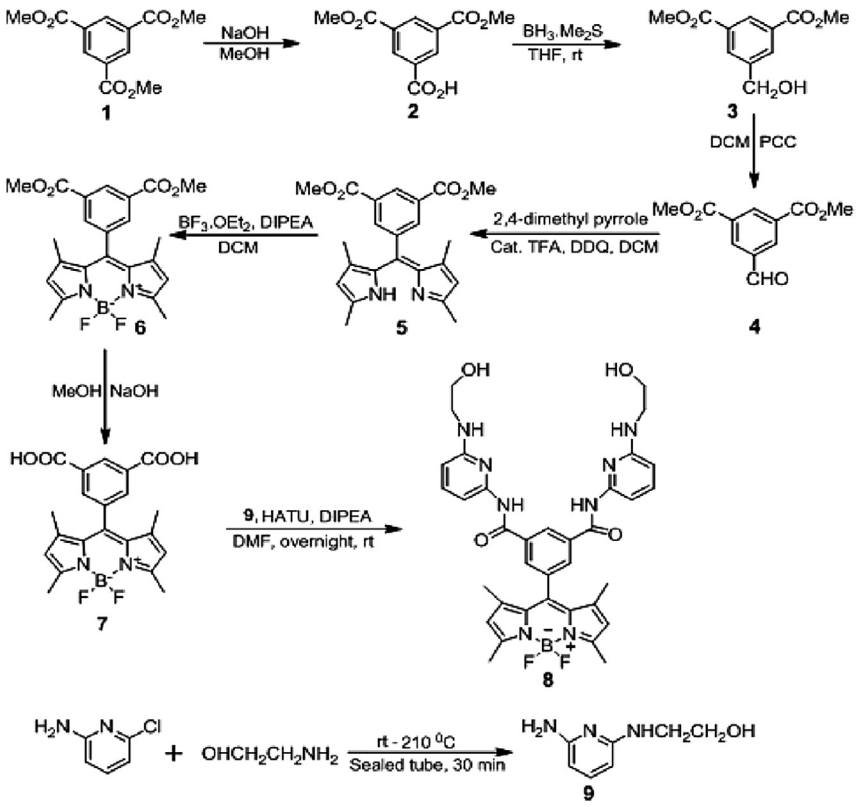

Scheme 1. Synthesis pathway of BODIPY-based fluorogenic probe **8**.

10.2 mmol) was added slowly and reaction was stirred overnight. After completion, the reaction quenched with brine, CH_2Cl_2 layer was separated, evaporated under reduced pressure and purified by column chromatography on silica gel (EtOAc:Hexane 1:9–3:7) to give compound **6** (110 mg, 65% yield) as a red sticky solid. ^{1}H NMR ($CDCl_3$, 300 MHz): δ 1.33 (s, 6H), 2.56 (s, 6H), 3.97 (s, 6H), 6.00 (s, 2H), 8.21 (s, 2H), 8.82 (s, 1H). ^{13}C NMR ($CDCl_3$, 100 MHz): 14.8, 14.9, 15.2, 52.9, 121.9, 131.4, 131.9, 133.8, 136.1, 142.8, 142.8, 156.6, 165.7 ppm. HRMS: Calculated for $C_{23}H_{23}BF_2N_2O_4$: 440.1719; found 440.1724.

2.2.6. Synthesis of 10-(3,5-dicarboxyphenyl)-5,5-difluoro-1,3,7,9-tetramethyl-5H-dipyrrolo[1,2-c:1′,2′-f][1,3,2]diazaborinin-4-ium-5-uide (7)

An aqueous solution of NaOH was added slowly to the solution of compound **6** (50 mg, 0.11 mmol) in 10 mL methanol and reaction was stirred for one day. The reaction mixture was neutralized by aqueous HCl solution, diluted with EtOAc. The organic solvent was separated and then removed under reduced pressure. The crude product was washed by ether two times to give the compound **7** (40 mg, 85% yield) as a dark red solid. ^{1}H NMR (CD_3OD, 300 MHz): δ 1.34 (s, 6H), 2.48 (s, 6H), 6.08 (s, 2H), 8.14 (s, 2H), 8.76 (s, 1H). ^{13}C NMR (CD_3OD, 100 MHz): 14.6, 15.0, 122.8, 132.3, 134.0, 134.6, 136.9, 157.5, 167.9 ppm. ESI-MS: Calculated for $C_{21}H_{19}BF_2N_2O_4$ (M+1) 412.14; found 413.31 (M+1).

2.2.7. Synthesis of 10-(3,5-bis(6-(2-hydroxyethylamino)pyridin-2-ylcarbamoyl)phenyl)-5,5-difluoro-1,3,7,9-tetramethyl-5H-dipyrrolo[1,2-c:1′,2′-f][1,3,2]diazaborinin-4-ium-5-uide (8)

To a stirred solution of compound **7** (50 mg, 0.12 mmol), HATU (115 mg, 0.30 mmol), and DIPEA (39 mg, 0.30 mmol) in dry DMF (5 mL) was added compound **9** (37 mg, 0.24 mmol). The reaction mixture was stirred at room temperature under argon atmosphere for 24 h. After completion of reaction, EtOAc and brine were added to the reaction mixture, EtOAc layer was separated and removed under reduced pressure to get the crude product which was purified by column chromatography (MeOH:DCM 0.5:9.5–2:9) to give final compound **8** (20 mg, 24% yield) as a dark red solid. ^{1}H NMR ($CDCl_3$, 400 MHz): δ 1.25 (s, 6H), 2.58 (s, 6H), 3.71 (t, J = 5.4 Hz, 4H), 4.16 (s, 2H), 4.49 (t, J = 5.4 Hz, 4H), 4.56 (s, 2H), 5.68 (d, J = 7.8 Hz, 2H), 5.79 (d, J = 7.9 Hz, 2H), 6.00 (s, 2H), 7.08 (t, J = 7.8 Hz, 2H), 8.00 (s, 2H), 8.75 (s, 1H). ^{13}C NMR ($CDCl_3$, 100 MHz): 14.9, 15.4, 40.8, 65.6, 96.2, 97.3, 121.9, 131.5, 131.8, 136.0, 139.5, 143.0, 156.5, 157.8, 158.0, 165.3 ppm. HRMS: Calculated for $C_{35}H_{37}BF_2N_8O_4$: 682.2999; found 705.2902 (M+Na).

2.2.8. Synthesis of 2-(6-aminopyridin-2-ylamino)ethanol (9)

A mixture of 6-chloropyridin-2-amine (500 mg, 3.90 mmol), and 2-aminoethanol (286 mg, 4.68 mmol) was heated for 1 h under neat condition in the sealed tube. DCM and brine were added to the reaction mixture and organic layer was separated, dried and removed under reduced pressure to get the crude product which was purified by column chromatography (MeOH:DCM 1:9–2:8) to give compound **9** (90 mg, 15% yield) as a dark green sticky liquid. ^{1}H NMR (DMSO-d_6, 300 MHz): δ3.32 (t, J = 5.5 Hz, 2H), 3.73 (t, J = 5.4 Hz, 2H), 4.66–4.67 (brs, 2H), 5.03 (s, 1H), 5.74–5.78 (m, 2H), 7.16 (t, J = 7.9 Hz, 1H). ^{13}C NMR (CD_3OD, 100 MHz): 42.6, 59.7, 93.7, 94.7, 137.9, 156.6 ppm. HRMS: Calculated for $C_7H_{11}N_3O$: 153.0902; found 154.0980 (M+1).

2.3. Theoretical calculations

Density Functional Theory (DFT) was used to optimize the geometry of compound **8** and **8**–uric acid. These were calculated at B3LYP/6-31G(d) level of theory. After vibration analysis of the optimized structures, we did not find any imaginary frequency,

which indicated that each of the optimized structures was at the real minimum on the potential energy surfaces (PES). For calculating interaction energy we corrected basis set superposition error (BSSE) by counterpoise correction method [30] applied on an optimized geometry. We defined the interaction energy (I.E) by the following relation (1), where $E_{comp.8}$ and E_{UA} are respectively optimized energies of compound **8** and uric acid, E_{BSSE}(dimer) indicates the dimeric system (**8**–uric acid) counterpoise corrected energy, $\Delta E_{\text{dimerization}}(corr.)$ is the corrected dimerization energy, which is the interaction energy or binding energy in this case.

$$I.E = \Delta E_{\text{dimerization}}(corr.) = E_{BSSE}(\text{dimer}) - (E_{comp.8} + E_{UA}) \quad (1)$$

We applied the time dependent density functional theory (TDDFT) to calculate the electronic excitation energies and oscillator strengths at B3LYP/6-31G(d) level of theory. All calculations were carried out using Gaussian 09 W program package [31].

2.4. Procedure for uric acid analysis by literature method

The ascorbic acid which interferes with detection of uric acid was removed from the samples by incubating samples with ascorbate oxidase. The samples were then subjected to react with uricase enzyme which converts uric acid into allantoin, CO_2 and H_2O_2. In the presence of peroxidase (POD), H_2O_2 reacts with N-ethyl-N-(2-hydroxy-3-sulfopropyl)-3-methylaniline (TOOS) and 4-aminophenazone to form a quinone-imine dye. The red colour intensity of this quinone-imine dye is proportional to the uric acid concentration and is determined photometrically.

$$\text{Uric Acid} + 2H_2O + O_2 \xrightarrow{\text{Uricase}} \text{Allantoin} + CO_2 + H_2O_2$$

$$H_2O_2 + H^+ + \text{TOOS} + \text{4-aminophenazone} \xrightarrow{\text{Peroxidase}} \text{Quinone-diimine dye} + 4H_2O$$

Reagents used for this analysis: Phosphate buffer: 0.05 mol/L, pH 7.8; TOOS: 7 mmol/L; fatty alcohol polyglycol ether: 4.8%; ascorbate oxidase (EC 1.10.3.3; zucchini; 25 °C) ≥ 83.5 μkat/L; potassium hexacyanoferrate (II): 0.30 mmol/L; 4-minophenazone ≥ 3 mmol/L; uricase (EC 1.7.3.3; Arthrobacter protophormiae; 25 °C) ≥ 83.4 μkat/L; peroxidase (POD) (EC 1.11.1.7; horseradish; 25 °C) ≥ 50 μkat/L.

3. Results and discussion

3.1. Theoretical calculations of probe *8* with uric acid

Prior to the synthesis of probe **8**, we carried out density functional theory (DFT) and time dependent density functional theory (TDDFT)-based calculations [31] to elucidate the interactions between probe **8** and UA at the molecular level. Fig. 1 shows the optimized structures of probe **8** and its UA complex (**8**–uric acid complex). Probe **8** binds to UA via its two flexible chelating units i.e. pyridinium arms through H-bonds. As predicted from theoretical calculations, the **8**–uric acid complex forms nearly 14 complementary H-bonds with each other (Fig. 1d). The H-bonds were defined by two geometric parameters [32,33]: the H···A distance <3.0 Å and the D–H···A angle >110° (Table S1, ESI). The calculated binding energy in the gas phase (−25.19 kcal/mol) indicates moderate interactions between probe **8** and UA. Average binding energy (calc.) for each H-bond is ~1.8 kcal/mol, which matched well with the H-bond energy revealed in the studies of barbiturate drug complexation with some synthetic hosts [27]. TDDFT calculations revealed that transitions from the ground state to the first singlet excited state in probe **8** are associated with the following excitations in molecular orbitals: HOMO-2 → LUMO, HOMO-1 → LUMO, and HOMO → LUMO (Table S2). The electron densities of HOMO-1 and HOMO-2 are located mainly in the chelating units, whereas in the case of HOMO and LUMO, they reside on the BODIPY unit (Figs. 2 and S1). This indicates that photo-induced electron transfer (or photo-induced charge transfer) may take place from the chelating unit to BODIPY, which accounts for the weak fluorescence property of probe **8**. When UA interacts with probe **8**, molecular orbitals HOMO, LUMO, and LUMO+1 are involved in the electronic transition (Table S2). Upon interaction with UA, the HOMO of probe **8** no longer resides on the chelating units and thus PET is no longer possible. The calculated oscillator strength increases from 0.05 to 0.202 (Table S2), indicating a probable increase in the absorbance of probe **8** in the visible spectra after chelating with UA. The above theoretical prediction motivated us to synthesize probe **8** and investigate it further.

3.2. Synthesis of probe *8*

Probe **8** was synthesized as shown in Scheme 1. The oxidation of compound **3** [29] with pyridinium chlorochromate (PCC) in dichloromethane gave dimethyl-5-formylisophthalate **4** in 16% yield. The reaction of compound **4** with 2,4-dimethylpyrrole in the presence of DDQ and TFA furnished **5**, which on reaction with $BF_3 \cdot OEt_2$ gave a BODIPY derivative, **6**. The hydrolysis of **6** to form **7** followed by HATU coupling with **9** yielded the required compound **8** (24% yield) as a dark red solid. All the compounds have been characterized and confirmed by ^{1}H NMR, ^{13}C NMR, ESI-MS, and HRMS (Figs. S2–S24).

3.3. Binding studies of probe *8* with uric acid

We investigated the photophysical behaviour and binding interactions of probe **8** with UA under physiological conditions (PBS

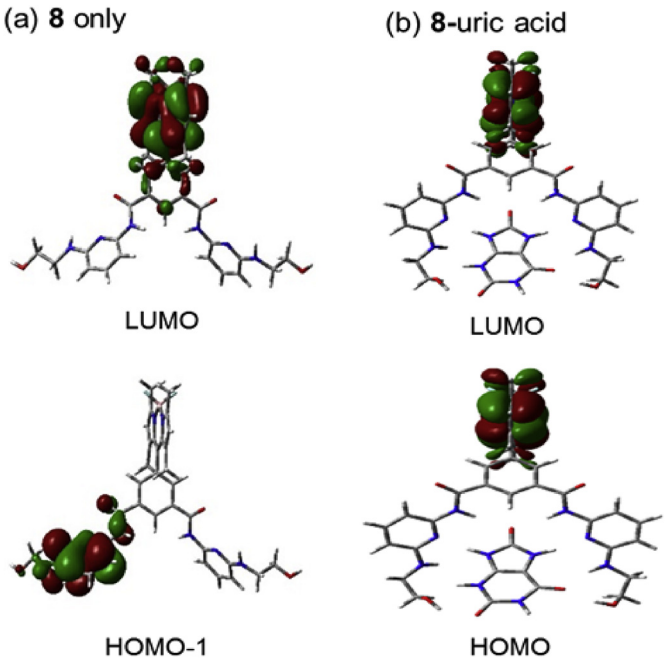

Fig. 2. Frontier molecular orbitals of (a) probe **8** and (b) **8**–uric acid. In the molecular orbitals representation, the different phases for the HOMOs and LUMOs are indicated by green, red, respectively and isovalue of 0.02 a.u. (For interpretation of the references to colour in this figure legend, the reader is referred to the web version of this article.)

buffer, pH 7.2, 37 °C) using UV–Vis and fluorescence spectroscopies. Compound **8** exhibited a weak absorption band at 507 nm (ε = 13666.7 M^{-1} cm^{-1}) in aqueous solution (Fig. 3). With the addition of UA (20 μM), an increase in the absorption was observed at 507 nm (ε = 23033.3 M^{-1} cm^{-1} Fig. 3). The change in the absorption indicates the binding of UA with probe **8**.

In the fluorescence spectra, probe **8** exhibits a weak emission band (ϕ_s = 0.004) at 510 nm when excited at 475 nm (Fig. 4). The weak fluorescence of probe **8** can be attributed to PET from amino-pyridine units to the BODIPY unit; this result is consistent with theoretical calculations. The fluorescence of probe **8** significantly enhanced (ϕ_s = 0.029) with the addition of UA (10–700 μM, Fig. 4) and showed a good linear relationship (Fig. S25). The enhancement in fluorescence emission induced by UA is due to the inhibition of PET from amino-pyridine units to the BODIPY unit. The stoichiometry of the probe **8** and UA was 1:1 evaluated by method of continuous variation (Job's plot, Fig. S26) using fluorescence changes of probe **8** with UA.

The selectivity of probe **8** towards UA was investigated by observing the changes in the fluorescence intensity at 512 nm in the presence of various bioanalytes such as xanthene, hypoxanthine, creatinine, ascorbic acid, cysteine, homocysteine, glutathione, glycine, L-tyrosine, L-arginine, L-glutamic acid, L-aspartic acid and L-serine in aqueous solution. Amongst all the analytes tested, probe **8** was found to be highly selective for UA (Fig. 5). Importantly, potentially competing analytes such as ascorbic acid (which cause strong interference in the electrochemical detection of uric acid due to very small difference in oxidation potentials of UA and AA), xanthene, hypoxanthine, and creatinine (which have the structural similarity with the uric acid) showed relatively insignificant change in the emission intensity of probe **8**. The complexation of probe **8** with UA was investigated as a function of pH and found to be quite stable over the biological pH range of 5–9 (Fig. S27), validating the utility of probe **8** under various biological conditions.

Prior to exploring the use of probe **8** in serum, it is important to calibrate fluorescence intensity changes with UA concentration. The fluorescence intensity of probe **8** increases with uric acid concentration (0–700 μM; Figs. S25 and S28) and the variation can be fitted with linear equation. We have used the correlation curve (Fig. S25) to estimate UA concentration in serum samples. This also indicates the high sensitivity of probe **8**, which is enough to detect UA at a 10 μM level under physiological environment. The UA concentration in serum was further quantified from eight different serum samples collected from normal humans, hyperuricemia, and hypouricemia patients. No pre-treatment of the serum samples was

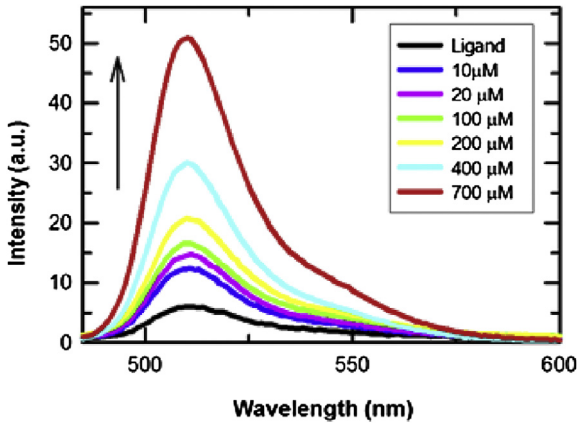

Fig. 4. Fluorescence spectra of probe **8** (6 μM, black line) with different concentrations of uric acid (0–700 μM, PBS solution, pH = 7.2). λ_{ex} = 475 nm, Slit: 3 nm/3 nm.

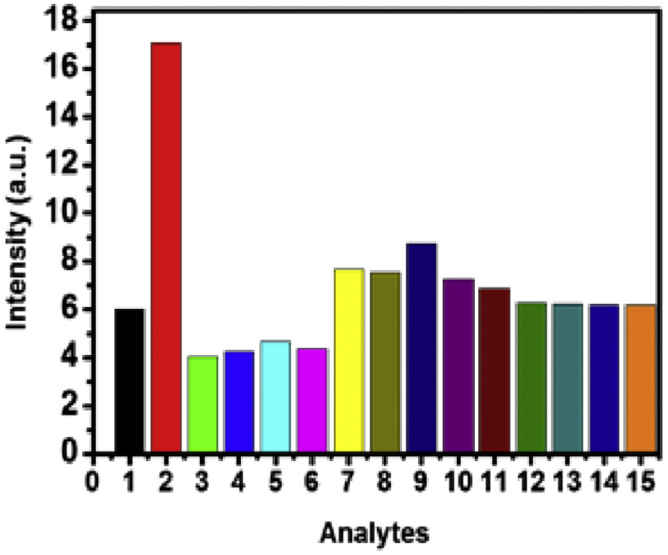

Fig. 5. Fluorescence changes of probe **8** (6 μM) in the presence of different analytes in aqueous solution (1. Probe **8** only, 2. Uric acid (100 μM), 3. Xanthene (100 μM), 4. Hypoxanthine (20 μM), 5. Creatinine (100 μM), 6. Ascorbic acid (100 μM), 7. Cysteine (100 μM), 8. Homocysteine (100 μM), 9. Glutathione (100 μM), 10. Glycine (100 μM), 11. L-tyrosine (100 μM), 12. L-arginine (100 μM), 13. L-glutamic acid (100 μM), 14. L-aspartic acid (100 μM), 15. L-serine (100 μM)). λ_{ex} = 475 nm, Slit: 3 nm/3 nm.

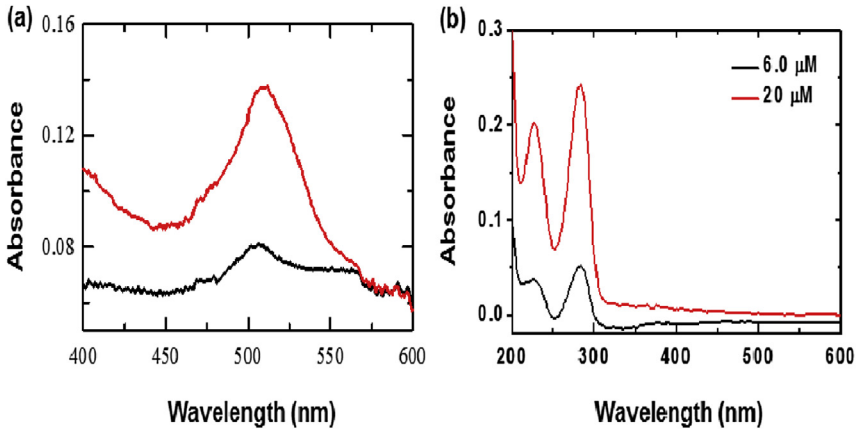

Fig. 3. Absorption spectrum of (a) probe **8** (6 μM, black solid line) and after addition of uric acid (20 μM, red solid line) and (b) uric acid only (6 μM and 20 μM PBS buffer, pH = 7.2). (For interpretation of the references to colour in this figure legend, the reader is referred to the web version of this article.)

Table 1
Uric acid concentration in serum samples. Comparison between a previously reported method and our method.

Sample No.	Literature method (μM)	Our method (μM)
1	773	>700 (917 ± 30)
2	666	630 ± 17
3	500	576 ± 12
4	476	469 ± 20
5	303	325 ± 15
6	196	217 ± 18
7	131	181 ± 21
8	63	145 ± 10

carried out for the quantification. The spectral profile of probe **8** in the presence of serum UA showed a significant increase in fluorescence intensity at 510 nm (Fig. S29), which is similar to fluorescence changes shown in Fig. 4. We subtracted the background fluorescence of serum samples from the fluorescence intensity of probe **8** to obtain the net fluorescence intensity for quantifying UA in serum samples (Table 1, Fig. S29). In order to compare our results with those reported in literature [34], we tested the same samples with The Roche Uric Acid Assay (current commercial method using Uric Acid Assay Kit). We found our method to be as efficient as the current commercial method for the determination of UA in serum (Table 1). However, the simplicity and non-enzymatic nature of our method make our probe well suited for clinical applications in the future.

4. Conclusions

We developed a highly selective non-enzymatic "turn-on" fluorescent probe for UA detection in serum samples. Probe **8** binds UA through several complementary H-bonds, which reduce PET from the chelating units to the BODIPY unit, resulting in "turn-on" fluorescence. Probe **8** has been found to be efficient in detecting a wide range of UA concentrations in serum samples (lower: ~60 μM, higher: ~700 μM and normal: ~120–380 μM). The detection limit and sensitivity of our method are similar to that of a commercial clinical analyser and could be useful in routine clinical and pharmaceutical analysis.

Acknowledgements

This work was supported by the CRI project (No. 2009-0081566) through the National Research Foundation of Korea.

Appendix A. Supplementary data

Supplementary data related to this article can be found at http://dx.doi.org/10.1016/j.dyepig.2015.05.001.

References

[1] Noroozifar M, Motlagh MK, Akbari R, Parizi MB. Simultaneous and sensitive determination of a quaternary mixture of AA, DA, UA and Trp using a modified GCE by iron ion-doped natrolite zeolite-multiwall carbon nanotube. Biosens Bioelectron 2011;28:56–63.
[2] Popa E, Kubota Y, Tryk DA, Fujishima A. Selective voltammetric and amperometric detection of uric acid with oxidized diamond film electrodes. Anal Chem 2000;72:1724–7.
[3] Klemp P, Stansfield SA, Castle B, Robertson MC. Gout is on the increase in New Zealand. Ann Rheum Dis 1997;56:22–6.
[4] Martinon F, Pétrilli V, Mayor A, Tardivel A, Tschopp J. Gout-associated uric acid crystals activate the NALP3 inflammasome. Nature 2006;440:237–41.
[5] Khosla UM, Zharikov S, Finch JL, Nakagawa T, Roncal C, Mu W, et al. Hyperuricemia induces endothelial dysfunction. Kidney Int 2005;67:1739–42.
[6] Daoussis D, Kitas GD. Uric acid and cardiovascular risk in rheumatoid arthritis. Rheumatology 2011;50:1354–5.
[7] Bos MJ, Koudstaal PJ, Hofman A, Witteman JCM, Breteler MMB. Uric acid is a risk factor for myocardial infarction and stroke. Stroke 2007;37:1503–7.
[8] Ullman B, Wormsted MA, Cohen MB, Martin DW. Purine oversecretion in cultured murine lymphoma cells deficient in adenylosuccinate synthetase: genetic model for inherited hyperuricemia and gout. Proc Natl Acad Sci 1982;79:5127–31.
[9] Yamanaka H, Togashi R, Hakoda M, Terai C, Kashiwazaki S, Dan T, et al. Optimal range of serum urate concentrations to minimize risk of gouty attacks during anti-hyperuricemic treatment. Adv Exp Med Biol 1998;431:13–8.
[10] Dinour D, Gray NK, Campbell S, Shu X, Sawyer L, Richardson W, et al. Homozygous SLC2A9 mutations cause severe renal hypouricemia. J Am Soc Nephrol 2010;21:64–72.
[11] Dehghan A, Hoek MV, Sijbrands EJG, Hofman A, Witteman JCM. High serum uric acid as a novel risk factor for type 2 diabetes. Diabetes Care 2008;31:361–2.
[12] Johnson RJ, Feig DI, Herrera-Acosta J, Kang D-H. Resurrection of uric acid as a causal risk factor in essential hypertension. Hypertension 2005;45:18–20.
[13] Goyal RN, Singhal NK. Comparison of electrochemical and enzymic oxidation of 1,3-dimethyluric acid. Bioelectrochem Bioenerg 1998;44:201–8.
[14] Odo J, Shinmato E, Shiozaki A, Hatae Y, Katayama S, Jiao G-S. Spectrofluorometric determination of uric acid and glucose by use of Fe(III)-thiacalix[4]arenetetrasulfonate as a peroxidase mimic. Health Sci 2004;50:594–9.
[15] Yu AM, Zhang HL, Chen HY. Catalytic oxidation of uric acid at the polyglycine chemically modified electrode and its trace determination. Analyst 1997;122:839–41.
[16] Zheng LZ, Wu SG, Lin XQ, Lei N, Rui L. Selective determination of uric acid by using a β-cyclodextrin modified electrode. Electroanalysis 2001;13:1351–4.
[17] Kabasakalian P, Kalliney S, Wescott A. Determination of uric acid in serum, with use of uricase and a tribromophenol-aminoantipyrine chromogen. Clin Chem 1973;19:522–4.
[18] Duncan PH, Grochman N, Cooper T, Smith E, Bayse D. A candidate reference method for uric acid in serum. I. Optimization and evaluation. Clin Chem 1982;28:284–90.
[19] Towne V, Will M, Oswald B, Zhao Q. Complexities in horseradish peroxidase-catalyzed oxidation of dihydroxyphenoxazine derivatives: appropriate ranges for pH values and hydrogen peroxide concentrations in quantitative analysis. Anal Biochem 2004;334:290–6.
[20] Li Y, Lin X. Simultaneous electroanalysis of dopamine, ascorbic acid and uric acid by poly (vinyl alcohol) covalently modified glassy carbon electrode. Sens Actuators B 2006;115:134–9.
[21] Lin X, Zhang Y, Chen W, Wu P. Electrocatalytic oxidation and determination of dopamine in the presence of ascorbic acid and uric acid at a poly (p-nitrobenzenazo resorcinol) modified glassy carbon electrode. Sens Actuators B 2007;122:309–14.
[22] Lin L, Chen J, Yao H, Chen Y, Zheng Y, Lin X. Simultaneous determination of dopamine, ascorbic acid and uric acid at poly (Evans Blue) modified glassy carbon electrode. Bioelectrochemistry 2008;73:11–7.
[23] Dey S, Saina D, Goswami S. Naphthyridine based fluorescent receptors for the recognition of uric acid. RSC Adv 2014;4:428–33.
[24] Chu H, Wei X, Wu M, Yan J, Tu Y. An electrochemiluminescent biosensor based on polypyrrole immobilized uricase for ultrasensitive uric acid detection. Sens Actuators B 2012;163:247–52.
[25] Chen D, Wang Q, Jin J, Wu P, Wang H, Yu S, et al. Low-potential detection of endogenous and physiological uric acid at uricase-thionine-single-walled carbon nanotube modified electrodes. Anal Chem 2010;82:2448–55.
[26] Valeur B, Bourson J, Pouget J, Czarnik AW. Fluorescent chemosensors for ion and molecule recognition. In: ACS symposium series 538. Washington, DC: American Chemical Society; 1993.
[27] Chang SK, Engen DV, Fan E, Hamilton AD. Hydrogen bonding and molecular recognition: synthetic, complexation, and structural studies on barbiturate binding to an artificial receptor. J Am Chem Soc 1991;113:7640–5.
[28] Loudet A, Burgess K. BODIPY dyes and their derivatives: syntheses and spectroscopic properties. Chem Rev 2007;107:4891–932.
[29] Haridas V, Sharma YK, Naik S. Multi-tier dendrimers with an aromatic core. Eur J Org Chem 2009:1570–7.
[30] Simon S, Duran M, Dannenberg JJ. How does basis set superposition error change the potential surfaces for hydrogen-bonded dimers? J Chem Phys 1996;105:11024–31.
[31] Frisch MJ, Trucks GW, Schlegel HB, Scuseria GE, Robb MA, Cheeseman JR, et al. Gaussian 09, revision B. 01. Wallingford, CT: Gaussian, Inc; 2010.
[32] Steiner T, Desiraju GR. Distinction between the weak hydrogen bond and the van der Waals interaction. Chem Commun 1998:891–2.
[33] Steiner T. The hydrogen bond in the solid state. Angew Chem Int Ed 2002;41:48–76.
[34] Kageyama N. A direct colorimetric determination of uric acid in serum and urine with uricase-catalase system. Clin Chim Acta 1971;31:421–6.